

# Wave Propagation in the Hot Duct of VHTR

ICONE 21

Jim C. P. Liou  
Richard R. Schultz

July 2013

The INL is a  
U.S. Department of Energy  
National Laboratory  
operated by  
Battelle Energy Alliance



This is a preprint of a paper intended for publication in a journal or proceedings. Since changes may be made before publication, this preprint should not be cited or reproduced without permission of the author. This document was prepared as an account of work sponsored by an agency of the United States Government. Neither the United States Government nor any agency thereof, or any of their employees, makes any warranty, expressed or implied, or assumes any legal liability or responsibility for any third party's use, or the results of such use, of any information, apparatus, product or process disclosed in this report, or represents that its use by such third party would not infringe privately owned rights. The views expressed in this paper are not necessarily those of the United States Government or the sponsoring agency.

## ICONE21 - 16807

### WAVE PROPAGATION in the HOT DUCT of VHTR

**Jim C. P. Liou\***

University of Idaho  
Moscow, Idaho 83844, USA

**Richard R. Schultz**

Idaho National laboratory  
Idaho Falls, Idaho 83415, USA

#### ABSTRACT

In VHTR, helium from the reactor vessel is conveyed to a power conversion unit through a hot duct. In a hypothesized Depressurized Conduction Cooldown event where a rupture of the hot duct occurs, pressure waves will be initiated and reverberate in the hot duct. A numerical model is developed to quantify the transients and the helium mass flux through the rupture for such events. The flow path of the helium forms a closed loop but only the hot duct is modeled in this study. The lower plum of the reactor vessel and the steam generator are treated as specified pressure and/or temperature boundary to the hot duct. The model is based on the conservation principles of mass, momentum and energy, and on the equations of state for helium. The numerical solution is based on the method of characteristics with specified time intervals with a predictor and corrector algorithm. The rupture sub-model gives reasonable results. Transients induced by ruptures with break area equaling 20%, 10%, and 5% of the duct cross-sectional area are described.

#### NOMENCLATURE

$A_b$  = area of a rupture oh duct wall;  
 $a$  = acoustic wave speed;  
 $c_p$  = specific heat at constant pressure;  
 $C_d$  = discharge coefficient of the rupture;  
 $D$  = diameter of hot duct;  
 $f$  = Darcy-Weisbach friction factor;  
 $g$  = gravitational acceleration;  
 $h$  = specific enthalpy of gas;  
 $h_{stg}$  = stagnation specific enthalpy of gas;  
 $K_0$  = constant along pathline (Eqs. 16 and 25);  
 $K_p$  = constant along C+ characteristic (Eqs. 17 and 26);  
 $K_n$  = constant along C- characteristic ( Eq. 18 and 27);  
 $L$  = length of hot duct;

$M$  = mach number;  
 $mb$  = mass flux through a rupture of duct wall;  
 $P$  = absolute pressure of gas;  
 $P_{atm}$  = absolute atmospheric pressure;  
 $q$  = heat transferred to gas;  
 $R$  = gas constant;  
 $s$  = specific entropy of gas;  
 $T$  = absolute gas temperature of gas;  
 $t$  = time;  
 $u$  = gas velocity;  
 $x$  = distance;  
 $\alpha$  = variable group defined by Eq. 14;  
 $\gamma$  = specific heat ratio;  
 $\theta$  = angle of the duct with horizontal;  
 $\rho$  = mass density of gas;  
 $\varphi$  = rate of  $P$  change with  $s$  at constant  $\rho$ ;  
 $\Delta x$  = computational reach length;  
 $\psi$  = variable group defined by Eq. 13;

#### INTRODUCTION

Research and development efforts are ongoing at universities, national laboratories, and commercial laboratories to study the behavior of Very High Temperature Reactor (VHTR) systems both at operational and accident conditions. VHTRs are of interest since they are capable of achieving very high exit temperature levels (around 1000°C at reactor exit) and correspondingly high operational efficiencies. The high exit temperatures are very useful for many process heat applications.

The VHTRs of interest are thermal reactors and generally have either prismatic or pebble-bed cores. An example of a typical helium cooled prismatic system design is shown in Fig. 1 (courtesy of General Atomics, Inc).

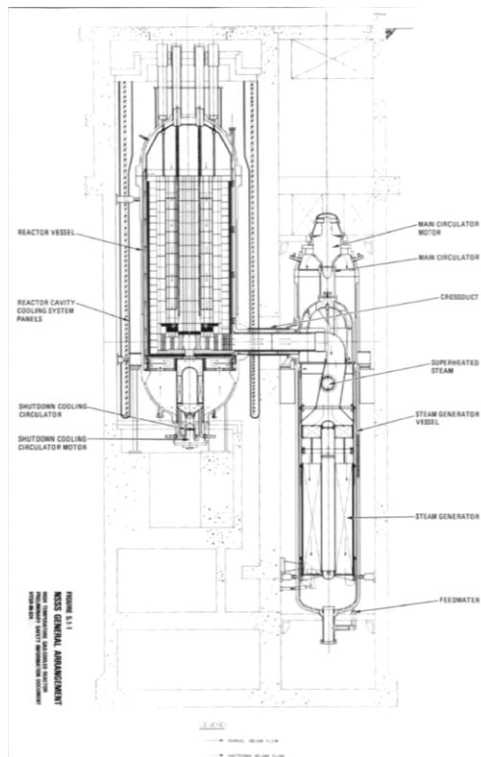


**Figure 1 System schematic (Source: Figure 5.1-1, NSSS General Arrangement, HTGR-86-024, Ref. 1)**

## SYSTEM DESCRIPTION

Referring to Fig. 1, the horizontal portion of the hot duct connects the reactor vessel on the left to the steam generator on the right. The hot duct penetrates the steam generator and connects to a bellows. It then turns downwards through an elbow and an extension. Reference 1 describes the helium flow path and the operating conditions of a VHTR. In summary, helium exits the lower plenum of the reactor vessel and enters the hot duct. After entering the steam generator, the hot duct transitions into a bellows, a downward-pointing elbow, and an extension section. The helium flows downwards into the steam generator, passes tube bundles, and then flows upwards through the passage in the wall of the steam generator toward a circulator located at the top of the steam generator. The circulator pumps the helium back to the inlet of the reactor core through an annular space around the hot duct and the cold channels in the wall of the reactor vessel. After passing through the core, the heated helium flows downwards toward the lower plenum and completes the flow loop.

Based on Fig. 1, the length of the hot duct, including the bellows, the elbow, and the extension is estimated to be 10.52 m. The diameter of the hot duct is 1.19 m. The hot duct is surrounded by a 3" thick thermal barrier. For a steady state operation at the rated reactor power, the mass flow rate of helium through the hot duct is 157.59 kg/s. According to Fig. 5.1-2 of HTGR-86-024, Ref. 1, the pressure and temperature at the reactor exit are 6.34 MPa absolute (919 psia) and 959.67 °K (1268 °F), respectively. The amount of helium in the reactor vessel (calculated by RELAP5 and provided by Richard Schultz) is 1276 kg. Additional helium mass is distributed in the rest of the system.

## METHOD OF APPROACH

The hot duct is idealized as a perfectly insulated horizontal conduit with a diameter of 1.19 m and a length of 10.52 m. The flow direction and duct elevation changes due to the elbow have no effect on pressure wave propagation and are ignored. The expansion in the extension has some effect but is ignored. This should result in slightly greater wave amplitudes. The pressure and temperature at the exit of the reactor core are assumed at the inlet of the hot duct. Duct wall rupture of various sizes is postulated to create transients. The pressures at the inlet and the outlet of the hot duct are held constant at their steady state values during transients. This is an acceptable approximation as long as the cumulated mass discharged through the rupture is small relative to the mass inventory of the reactor system. The flow into the duct (from either end) is assumed to be isentropic (i.e., no head loss) but the frictional energy loss is modeled.

A numerical model based on the method of characteristics for one dimensional gas dynamics has been developed. The validity of this model is then checked with the analytical solution of a shock tube problem. Transients induced by ruptures of various sizes (one rupture for each scenario) at the mid-length and at quarter-length from the hot duct outlet were simulated. Details of the model development, partial validation, and results are given below.

## GOVERNING EQUATIONS

The conservation equations of mass, momentum, and energy and the equation of state of the gas form the basis of the numerical model. Entropy generation due to the flow resistance of the duct, heat conduction through duct wall, and any slope of the duct, if any, are modeled.

The governing equations are (2, 3),

$$\left(\frac{\partial \rho}{\partial t} + u \frac{\partial \rho}{\partial x}\right) + \rho \frac{\partial u}{\partial x} = 0 \quad (1)$$

$$\rho \frac{\partial u}{\partial t} + \rho u \frac{\partial u}{\partial x} = -\frac{\partial P}{\partial x} - \rho g \sin \theta - \frac{f \rho u |u|}{2D} \quad (2)$$

$$\rho \left( \frac{\partial h}{\partial t} + u \frac{\partial h}{\partial x} \right) - \left( \frac{\partial P}{\partial t} + u \frac{\partial P}{\partial x} \right) = q + \frac{f \rho |u|^3}{2D} \quad (3)$$

in which  $\theta$  = the angle of the duct with the horizontal, positive when the duct is tilted upwards,  $D$  = the diameter of the duct,  $f$  = Darcy-Weisbach friction factor,  $g$  = gravitational acceleration,  $h$  = specific enthalpy of the gas,  $u$  = gas velocity, and  $q$  = the heat transferred to the gas through duct wall on a per unit volume basis. The fourth governing equation needed for the four variables  $\rho$ ,  $u$ ,  $P$ , and  $h$  is an equation of state.

Helium, as a noble gas and at pressure and temperature encountered in helium cooled reactors, behaves as a perfect gas (4). Consequently, the following relations hold (5, 6).

$$P = \rho R T \quad (4)$$

$$h = \frac{\gamma}{\gamma - 1} \frac{P}{\rho} \quad (5)$$

$$a = \sqrt{\left(\frac{\partial P}{\partial \rho}\right)_s} = \sqrt{\frac{\gamma P}{\rho}} \quad (6)$$

$$\left(\frac{\partial P}{\partial s}\right)_\rho = \frac{\gamma P}{c_p} \quad (7)$$

in which  $a$  = acoustic wave speed,  $R$  = gas constant,  $T$  = absolute temperature,  $s$  = specific entropy, and  $\gamma$  = specific heat ratio.

By viewing  $P$  as a function of  $\rho$  and  $s$ , and with the use of Eq. 7 and the thermodynamic relationship,

$$dh = T ds + \frac{dP}{\rho} \quad (8)$$

the terms in the bracket on the left side of Eq. 1, which represents the total derivative of mass density along fluid particle path, can be written as (7)

$$\begin{aligned} \frac{d\rho}{dt} &= \frac{1}{a^2} \left( \frac{dP}{dt} \left( 1 + \frac{\phi}{\rho T} \right) - \frac{\phi}{T} \frac{dh}{dt} \right) \quad \text{with } \phi \\ &= \left( \frac{\partial P}{\partial s} \right)_\rho = \frac{\gamma P}{c_p} \end{aligned} \quad (9)$$

Using Eq. 9, the equation for mass conservation (Eq. 1) becomes (7)

$$(\rho T + \phi) \frac{dP}{dt} - \rho \phi \frac{dh}{dt} + \rho^2 a^2 T \frac{\partial u}{\partial x} = 0 \quad (1a)$$

Equations 1a, 2, and 3 constitute the set of governing equations for the numerical model. Note that the original three conservation equations involve derivatives in all four dependent variables  $\rho$ ,  $u$ ,  $P$ , and  $h$ . Substituting Eq. 9 into Eq. 1, the derivative in  $\rho$  is eliminated. Reference 8 claims that this reformulation improves accuracy of the numerical model.

Equations. 1a, 2 and 3 form a hyperbolic system and are transformed into a set of three ordinary differential equations along three characteristic lines in the  $x - t$  plane (9)

$$C0: \quad \rho \frac{dh}{dt} - \frac{dP}{dt} = \psi \quad \text{along} \quad \frac{dx}{dt} = u \quad (10)$$

$$C+: \quad \frac{dP}{dt} + \rho a \frac{du}{dt} = \frac{\phi \psi}{\rho T} + a \alpha \quad \text{along} \quad \frac{dx}{dt} = u + a \quad (11)$$

$$C-: \quad \frac{dP}{dt} - \rho a \frac{du}{dt} = \frac{\phi \psi}{\rho T} - a \alpha \quad \text{along} \quad \frac{dx}{dt} = u - a \quad (12)$$

where

$$\psi = q + \frac{f \rho |u|^3}{2D} \quad (13)$$

$$\alpha = -\rho g \sin \theta - \frac{\rho f u |u|}{2D} \quad (14)$$

Since the modeled hot duct is insulated and horizontal,  $q = 0$  and  $\theta = 0$ .

## METHOD OF CHARACTERISTICS

A specified time intervals is used in the method of characteristics. The duct is divided into a number of computational reaches of equal length  $\Delta x$ . The size of the time step is bound by the Courant-Friedrichs-Lewy condition to ensure numerical stability,

$$\Delta t \leq \frac{\Delta x}{|u + a|_{\max}} \quad (15)$$

Figure 2 shows the computational grid at an interior point. The solution at time  $t$  is known and the solution at  $t + \Delta t$  is sought. At point  $j$ , there exist a C+ characteristic that extends backwards in time and intersects the time =  $t$  line at point  $p$ . Similarly, a C- characteristic is extended backwards from  $j$  to  $n$  and, and a C0 characteristic is extended backwards from  $j$  to  $\theta$ . Because  $u$  and  $a$  are unknown at  $j$ , the slope of the characteristics are unknown must be approximated. A predictor and corrector method (2) is used to overcome this problem.

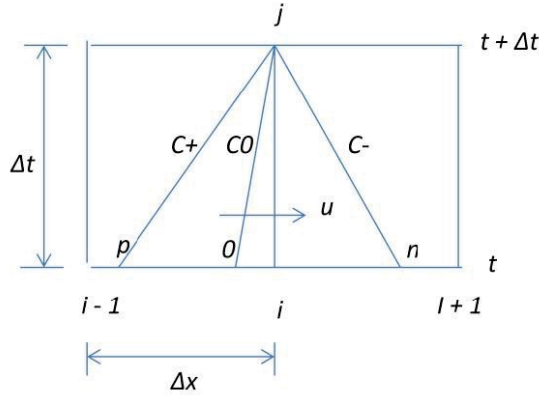


**Figure 2 Characteristics at a representative interior point. The pathline C0 shown is for a positive flow (left to right). For negative flow, point  $\theta$  is located between  $x_i$  and  $x_{i+1}$**

### The Predictor

For the predictor, the locations of points  $p$ ,  $\theta$ , and  $n$  are found by linearly interpolations from the known solutions at grid points  $(x_{i-1}, t)$ ,  $(x_i, t)$ , and  $(x_{i+1}, t)$ . This is done by assuming each characteristic has a constant slope (i.e., straight-line characteristic) computed by  $u + a$  at  $p$  for the C+ characteristic,  $u - a$  at  $n$  for the C- characteristic, and  $u$  at  $\theta$  for the C0 characteristic or the pathline. The compatibility equations are approximated as

$$C0: \rho_0(h_j - h_0) - (P_j - P_0) = \psi_0 \Delta t = K_0^1 \quad (16)$$

$$C+: (P_j - P_p) + (\rho a)_p(u_j - u_p) = \left( \frac{\phi \psi}{\rho T} + a \alpha \right)_p \Delta t = K_p^1 \quad (17)$$

$$C-: (P_j - P_n) - (\rho a)_n(u_j - u_n) = \left( \frac{\phi \psi}{\rho T} - a \alpha \right)_n \Delta t = K_n^1 \quad (18)$$

From these, a set of tentative value for  $u_j$ ,  $P_j$  and  $h_j$  are found as

$$u_j = \frac{K_p^1 - K_n^1 + (\rho a)_p u_p + (\rho a)_n u_n + P_p - P_n}{(\rho a)_p + (\rho a)_n} \quad (19)$$

$$P_j = K_p^1 - (\rho a)_p(u_j - u_p) + P_p \quad (20)$$

$$h_j = h_0 + \frac{K_0^1 + P_j - P_0}{\rho_0} \quad (21)$$

### The Corrector

Next, the locations of  $p$ ,  $\theta$ , and  $n$  are re-evaluated using the slope of the characteristics based on  $u_j$ ,  $a_j$  and the values of  $u$  and  $a$  at  $p$ ,  $\theta$ , and  $n$  as follows,

$$C0: x_j - x_0 = \frac{u_j + u_0}{2} \Delta t \quad (22)$$

$$C+: x_j - x_p = \frac{u_j + a_j + u_p + a_p}{2} \Delta t \quad (23)$$

$$C-: x_j - x_n = \frac{u_j - a_j + u_n - a_n}{2} \Delta t \quad (24)$$

Once the  $x_p$ ,  $x_0$ , and  $x_n$  are solved from Eqs 22, 23, and 24, we can find  $u$ ,  $P$  and  $h$  at  $p$ ,  $\theta$ , and  $n$  by linear interpolation the  $u$ ,  $P$ , and  $h$  at grid points  $(x_{i-1}, t)$ ,  $(x_i, t)$ , and  $(x_{i+1}, t)$ . The compatibility equations are now approximated by,

$$C0: \frac{\rho_0 + \rho_j}{2}(h_j - h_0) - (P_j - P_0) = \frac{\psi_0 + \psi_j}{2} \Delta t = K_0^2 \quad (25)$$

$$C+: (P_j - P_p) + \frac{(\rho a)_j + (\rho a)_p}{2}(u_j - u_p) = \frac{\left( \frac{\phi \psi}{\rho T} + a \alpha \right)_j + \left( \frac{\phi \psi}{\rho T} + a \alpha \right)_p}{2} \Delta t = K_p^2 \quad (26)$$

$$C-: (P_j - P_n) - \frac{(\rho a)_j + (\rho a)_n}{2} (u_j - u_n) \\ = \frac{\left( \frac{\phi \psi}{\rho T} - a\alpha \right)_j + \left( \frac{\phi \psi}{\rho T} - a\alpha \right)_n}{2} \Delta t = K_n^2 \quad (27)$$

Eliminate  $P_j$  between Eqs. 26 and 27 to obtain a new value for  $u_j$

$$u_j = \frac{K_p^2 - K_n^2 + \frac{1}{2} [(\rho a)_j + (\rho a)_p] u_p + \frac{1}{2} [(\rho a)_j + (\rho a)_n] u_n + P_p - P_n}{\frac{1}{2} [(\rho a)_j + (\rho a)_p + (\rho a)_j + (\rho a)_n]} \quad (28)$$

Use this new  $u_j$ , a new  $P_j$  is found from Eq. 26

$$P_j = K_p^2 - \frac{1}{2} [(\rho a)_j + (\rho a)_p] (u_j - u_p) + P_p \quad (29)$$

and a new value for  $h_j$  is found from Eq. 25

$$h_j = h_0 + \frac{K_0^2 + P_j - P_0}{\frac{\rho_j + \rho_0}{2}} \quad (30)$$

This completes one iteration. Using the newly found  $u_j$ ,  $P_j$  and  $h_j$ , we adjust the average slope of the characteristics again to compute yet another set of new  $u_j$ ,  $P_j$  and  $h_j$ . The iteration continues until convergence is achieved. In this fashion,  $u$ ,  $P$ , and  $h$  can be found at all interior points at time  $t + \Delta t$ . At each point, the mass density is computed from the known  $P$  and  $h$  using Eq. 22. The wave speed is then computed from the known  $P$  and  $\rho$  using Eq. 23, and the temperature is computed from the known  $P$  and  $\rho$  using Eq. 21.

## THE INITIAL CONDITION

A steady state adiabatic flow with friction is used as the initial condition. Knowing the pressure, temperature at the inlet and the steady state mass flow rate, the gas velocity  $u(0)$  and the Mach number  $M$  at the inlet can be computed. The gas velocity  $u(x)$  at  $x$  distance from the inlet can be computed from (2)

$$\frac{fx}{D} = \frac{1}{\gamma M^2} \left( 1 + \frac{\gamma-1}{2} M^2 \right) \left[ 1 - \left( \frac{u(0)}{u(x)} \right)^2 \right] + \frac{\gamma+1}{2\gamma} \ln \left( \frac{u(0)}{u(x)} \right)^2 \quad (31)$$

The pressure  $P(x)$  along the duct is computed next after knowing  $u(x)$

$$\frac{P(x)}{P(0)} = \frac{u(0)}{u(x)} \left\{ 1 + \frac{\gamma-1}{2} M^2 \left[ 1 - \left( \frac{u(x)}{u(0)} \right)^2 \right] \right\} \quad (32)$$

The mass density  $\rho(x)$  is computed from the continuity equation

$$\rho(x) = \rho(0) \frac{u(0)}{u(x)} \quad (33)$$

The specific enthalpy and wave speed can be computed from the known pressure and mass density using Eqs. 5 and 6.

Lastly, the stagnation enthalpy at the inlet and outlet are computed as

$$hstg_0 = h(0) + \frac{u(0)^2}{2} \quad (34)$$

$$hstg_L = h(L) + \frac{u(L)^2}{2} \quad (35)$$

in which  $L$  is the length of the duct. These stagnation enthalpies are needed in defining the boundary conditions at the inlet and the outlet of the duct.

## THE BOUNDARY CONDITIONS

Three boundary conditions are necessary. These are: specified pressure at the duct inlet, specified pressure at the duct outlet, and rupture on the duct wall.

### Boundaries with Specified Pressure

Figure 3 shows the possible situations at these boundaries. The details are given for the inlet. The outlet boundary is treated in a similar manner.

The primary unknowns at the upstream boundary are the velocity and enthalpy of the gas. Depending on the direction of flow, two possibilities exist as shown in Fig. 3. Let  $PP_0$  represent the specified inlet pressure and  $uP_0$  the unknown gas velocity at the inlet. In the predictor and for forward flow, the compatibility equation along the C- characteristic provides the equation to compute a tentative  $uP_0$

$$uP_0 = u_n + \frac{PP_0 - P_n - K_n^1}{(\rho a)_n} \text{ along } x_0 - x_n = u_n \Delta t \quad (36)$$

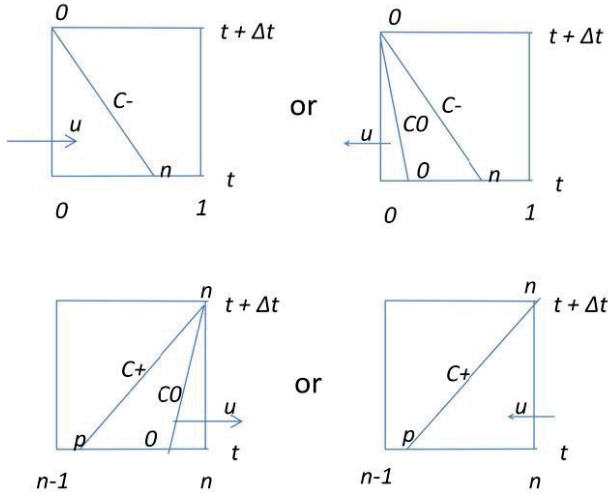


**Figure 3** Boundary conditions at the inlet (top row) and outlet (bottom row) of the hot duct. The availability of the compatibility equation along the pathline depends on whether the flow is positive (left column) and negative (right column)

The corrector is activated next. If this tentative  $uP_0$  is positive, then use it together with  $PP_0$  and the stagnation enthalpy at the inlet  $hstg_0$  to compute tentative values of mass density and specific enthalpy at the inlet assuming isentropic inflow (6)

$$\rho P_0 = \frac{\gamma}{\gamma-1} \frac{PP_0}{hstg_0 - \frac{uP_0^2}{2}} \quad (37)$$

$$hP_0 = \frac{\gamma}{\gamma-1} \frac{PP_0}{\rho P_0} \quad (38)$$

If the tentative  $uP_0$  is negative, then there is a C0 characteristic emanating from the duct interior to the inlet. The compatibility equation of this characteristic is used to obtain

$$hP_0 = h_0 + \frac{K_0^2 + PP_0 - P_0}{\frac{\rho_0 + \rho P_0}{2}} \quad (39)$$

$$\rho P_0 = \frac{\gamma}{\gamma-1} \frac{PP_0}{hP_0} \quad (40)$$

Next, the tentative values of gas velocity and wave speed (computed from the known pressure and mass density using Eq. 20) at the inlet are used to update the

position of point  $n$  and  $0$  (if the flow is still negative). The gas velocity, pressure, and specific enthalpy at points  $n$  and  $0$  (if applicable) are then interpolated using the known values on the first two grid points at time level  $t$ . The gas velocity is computed again for the corrector from

$$uP_0 = u_n - \frac{K_n^2 - PP_0 + P_n}{\frac{(\rho a)_n + \rho P_0 a P_0}{2}} \quad (41)$$

The corrector computations are repeated until the computed  $uP_0$  converges.

The algorithm at the outlet boundary is essentially the same except that the C- characteristic and its compatibility equation are replaced by a C+ characteristic and its compatibility equation.

### Serial Junction with a Break

The fluid dynamic aspects of a rupture of duct wall are modeled as a serial junction that allows flow leaving the duct at the junction. There are three possible situations which are shown in Fig. 4. In the top panel, gas escapes the hot duct from both directions. In the middle panel, break flow occurs while the through flow in the duct at the break location is positive. In the lower panel, the break flow exists while the through flow in the duct is negative. Modeling all these conditions requires different considerations.

Let  $iu$  and  $id$  denote the section immediately upstream and downstream of the break at time  $t$ . Let  $ju$  and  $jd$  denote the same sections at  $t+\Delta t$ . When the break flow comes from both directions, the specific enthalpy and mass density at  $ju$  and  $jd$  will be different. There are 7 unknowns: junction pressure  $PP_j$ , junction mass density,  $\rho P_j$ , gas velocities  $uP_{ju}$  and  $uP_{jd}$ , specific enthalpy  $hP_{ju}$  and  $hP_{jd}$ , and the break mass flow rate  $mb$ . The available equations are:

1. The compatibility equation along the C+ characteristic

$$uP_{ju} = u_p + \frac{K_p^2 - PP_j + P_p}{\frac{(\rho a)_p + (\rho P_{ju} a P_{ju})}{2}} \quad (42)$$

2. The compatibility equation along the C- characteristic

$$uP_{jd} = u_n - \frac{K_n^2 - PP_j + P_n}{\frac{(\rho a)_n + (\rho P_{jd} a P_{jd})}{2}} \quad (43)$$

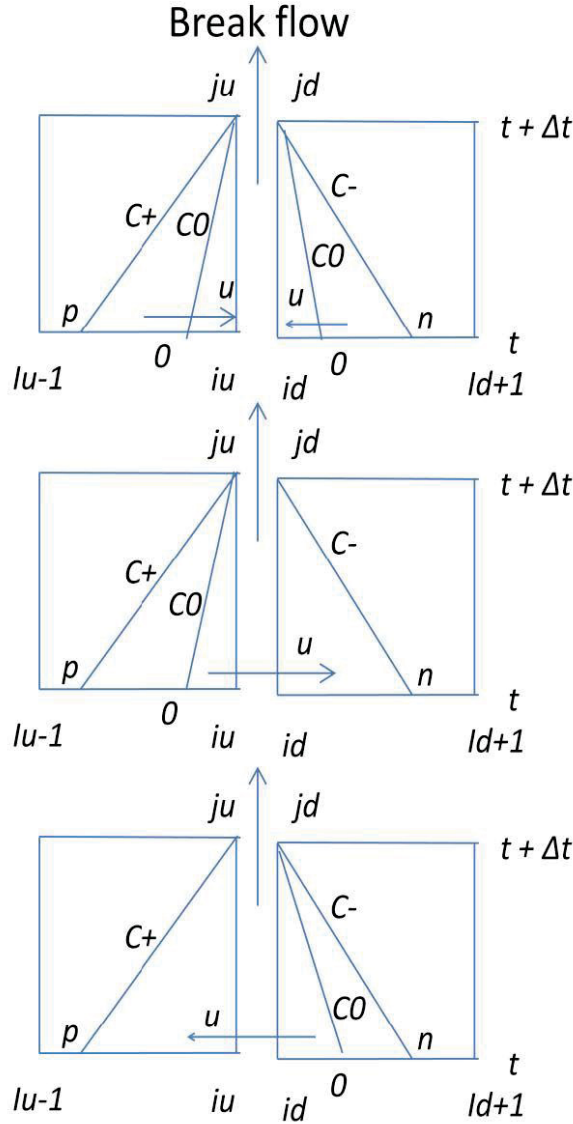


**Figure 4 The structure of the characteristics at a serial junction where a break may exist.**

3. The compatibility equation along the C0 from upstream

$$hP_{ju} = h_{0_{left}} + \frac{K_{0_{left}}^2 + PP_j - P_{0_{left}}}{\frac{\rho_{0_{left}} + \rho P_{ju}}{2}} \quad (44)$$

4. The compatibility equation along the C0 characteristic from downstream

$$hP_{jd} = h_{0_{right}} + \frac{K_{0_{right}}^2 + PP_j - P_{0_{right}}}{\frac{\rho_{0_{right}} + \rho P_{jd}}{2}} \quad (45)$$

5. Junction mass density

$$\rho P_j = \frac{\rho P_{ju} |uP_{ju}| + \rho P_{jd} |uP_{jd}|}{|uP_{ju}| + |uP_{jd}|} \quad (46)$$

6. Break flow equation (Wylie and Streeter 1993)

For subsonic efflux when  $\frac{P_{atm}}{\left(\frac{2}{\gamma+1}\right)^{\frac{\gamma}{\gamma-1}}} > PP_j > P_{atm}$

$$mb = C_d A_b \sqrt{2 \rho P_j PP_j^{\frac{\gamma}{\gamma-1}} \left(\frac{PP_j}{P_{atm}}\right)^{\frac{2}{\gamma}} \left[1 - \left(\frac{PP_j}{P_{atm}}\right)^{\frac{\gamma-1}{\gamma}}\right]} \quad (47)$$

For choked efflux when  $PP_j > \frac{P_{atm}}{\left(\frac{2}{\gamma+1}\right)^{\frac{\gamma}{\gamma-1}}}$

$$mb = \frac{C_d A_b}{\sqrt{RT}} \sqrt{\gamma \left(\frac{2}{\gamma+1}\right)^{\frac{\gamma+1}{\gamma-1}}} \quad (48)$$

7. Junction continuity equation

$$\left( \frac{\rho P_{ju} u P_{ju} + \rho_{iu} u_{iu}}{2} - \frac{\rho P_{jd} u P_{jd} + \rho_{id} u_{id}}{2} \right) A = \frac{mb_{t+\Delta t} + mb_t}{2} \quad (49)$$

When the break flow is supplied from one direction only,  $hP_{ju} = hP_{jd}$  and only the C0 compatibility equation from the upwind is available. In addition, the junction specific enthalpy and mass density come from the upwind direction.

The unknowns are solved by a trial and error process. The left and right sides of the continuity are computed separately based on a guessed junction pressure. Let the difference between the two sides be the residue. The process of driving the residue to zero is formulated as a root-finding problem. The Newton's iteration method is

employed successfully to find the correct junction pressure. The remaining unknowns are then computed from the equations provided above.

#### A CHECK ON THE NUMERICAL MODEL

Analytical solutions to the modeling equations exist for inviscid flow free from the influence of boundaries. The numerical model is checked against such a solution.

Consider a shock tube where a diaphragm separates the tube into two halves. Initially, the stagnant gas in left half has a pressure of 1 MPa and a mass density of  $1 \text{ kg/m}^3$ . The same gas on the right is also stagnant but has a pressure of 0.7 MPa and a mass density of  $0.5 \text{ kg/m}^3$ . The computed velocity, pressure, and mass density at  $t = 3.047 \times 10^{-3}$  seconds are compared with the analytical solution in Fig. 5. It is seen that there is some smearing at the expansion fan and across the jump mass discontinuity. The position of the pressure wave front is over-predicted slightly. These inaccuracies are inherent to the interpolations used in the specified time implementation of the method of characteristics. The velocity, pressure, and the mass densities between the pressure wave front and the tail of the expansion fan are predicted accurately. Given the very significant discontinuity in pressure and mass density in the initial condition, the agreement between the numerical (using 200 computational reaches) and analytical solutions is considered acceptable.

#### WAVES AND BREAK FLOWS IN THE HOT DUCT SUBSEQUENT TO A RUPTURE

Ruptures of duct wall with sizes of 20, 10, and 5 percent of the cross-sectional area of the hot duct were postulated at the mid-length and at quarter-length from the duct outlet were simulated. Two hundred computational reaches were used to keep numerical diffusion minimal. In each case, a Darcy-Weisbach friction factor of 0.029, computed from the steady state, was used. The friction factor should not influence the results strongly due to the short length of the duct. A discharge coefficient of 0.6 was used to account for the energy loss for the flow through the break. This is a realistic value and typically used in modeling air relief valves, a situation not unlike the flow through a break. The pressure in the containment is atmospheric.

Figure 6 shows the time trace of velocity and absolute pressure for a 20% rupture at the mid-length of the duct. The solid red and blue lines indicate the values at the inlet and the outlet of the duct. The dotted red and blue lines indicate the values immediately to the left and right of the break, respectively.

At the break location and prior to the break, the local pressure and velocity are 6.34 MPa and 44.6 m/s. The

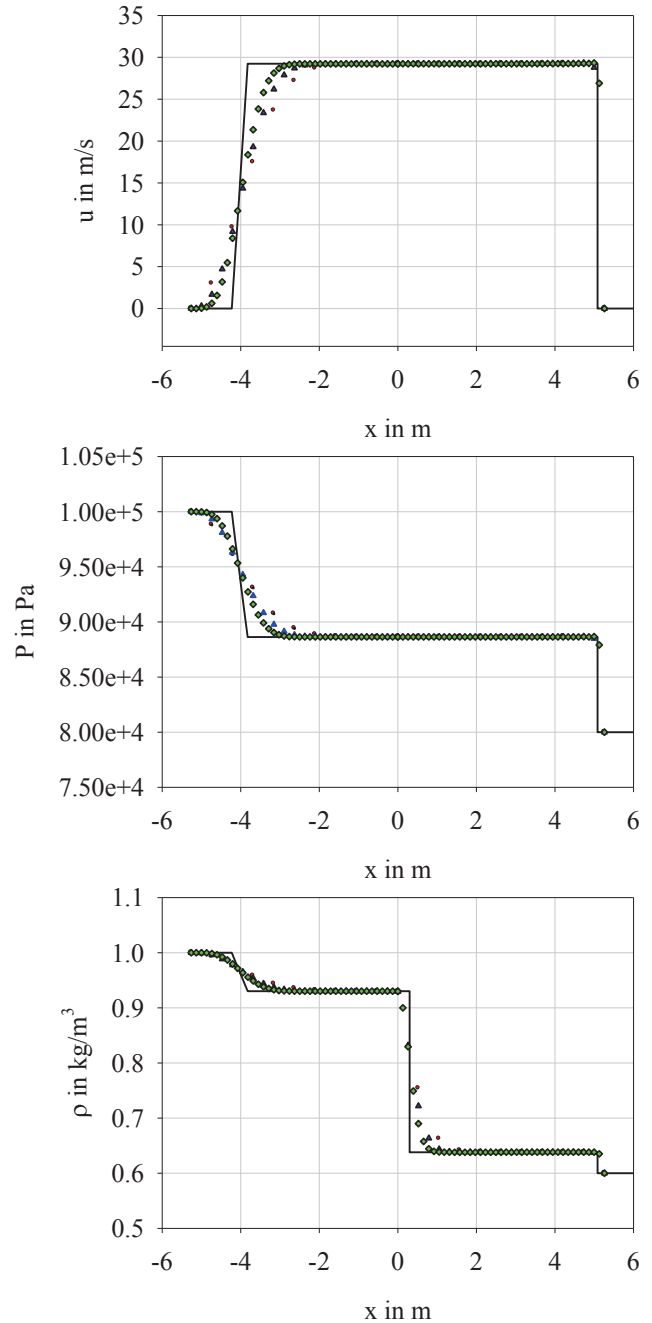


**Figure 5 Comparison with an analytical solution of an initial value problem of a shock tube (solid line) with 20 (circle), 40 (triangle), and 80 (diamond) computational reaches in the numerical model**

Break causes an immediate local depressurization from 6.34 to 5.98 MPa. With the depressurization, the pressure at the break is still much higher than the ambient and helium is drawn from both sides of the break and discharges out through the break as a choked

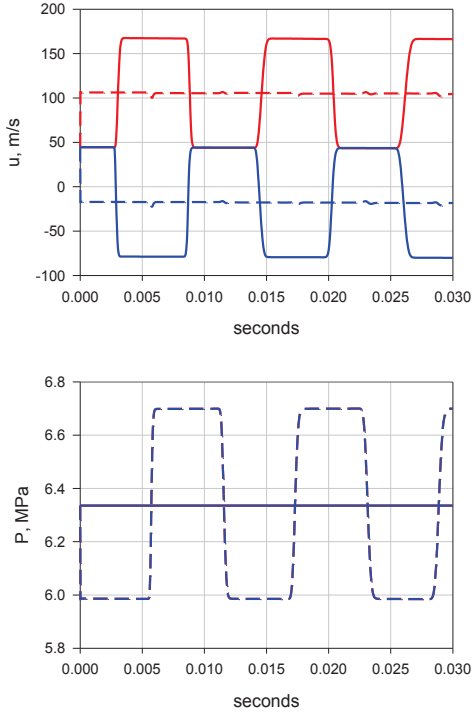


**Figure 6 Velocity and pressure variations induced by a 20% break at mid-length of hot duct**

flow. The velocity right after the break is 106.8 m/s on the left side and -17.7 m/s on the right side.

The depressurization propagates out in both directions as waves. The waves reach the inlet and the outlet at about 0.028 s and additional flow is drawn into the duct from both ends. This is evidenced by the velocity increase from the initial 44.6 m/s to 167 m/s at the inlet and the velocity decrease from 44.7 m/s to -78.8 m/s, both occurring at 0.0028 s. The reflected waves from the boundaries bring additional flows and the boundary pressures (6.34 MPa) back to the break location. Upon arrival at about 0.0056 (0.0028x2) s, the waves collide at the break location and cause an additional pressure rise, resulting in a peak pressure of 6.70 MPa. This peak pressure persists for 0.0056 s. At that time, the waves reflected from the boundaries bring the pressure down to 5.98 MPa. It took 0.0028x4 or 0.0112 s to complete one cycle of oscillation. The cycle repeats itself with little damping since the frictional resistance to flow is small on account of the short length of the duct.

Figure 7 shows the mass density and absolute temperature variations at the same locations as in Fig. 6. The slightly higher mass density during periods of high inflow gas velocity is due to the assumption of constant inlet pressure and isentropic inflow. Both the mass density and the absolute temperature vary according to pressure and exhibit the same periodic variations.

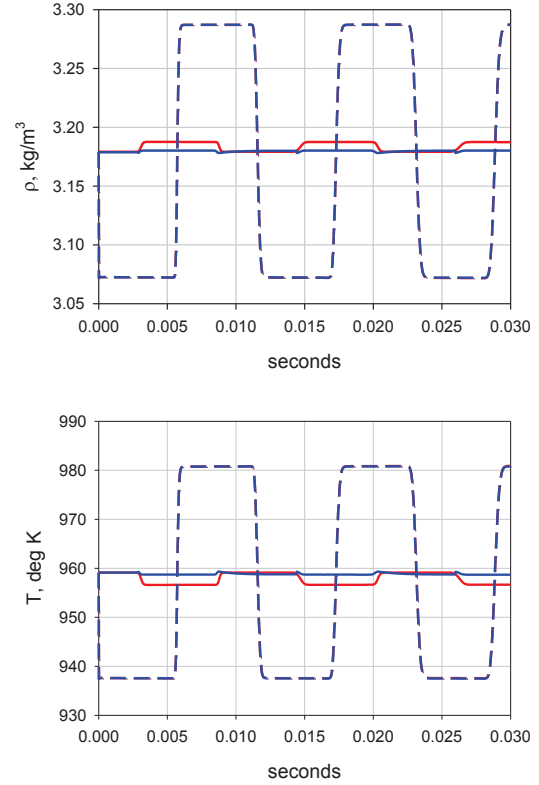


**Figure 7 Mass density and temperature variations induced by a 20% break at mid-length of hot duct**

The top panel of Fig. 8 shows the break mass flow rate and the cumulative mass discharged through the break over time. The break flow rate initially initiated is 420 kg/s. Thereafter, there is a slight variation according to the pressure oscillations at the break location. At 0.03 s or about 2.6 cycles of oscillations, the mass of gas discharged is approximately 13 kg. This is a very small amount compared with the total helium inventory in the system. Therefore, the assumption of constant pressure and constant specific stagnant enthalpy boundary conditions is justified. The bottom panel of Fig. 8 shows the rate of helium mass inventory change inside the hot duct. It varies in step with pressure as expected. Long term simulations show that the mass inventory change approaches zero as a new steady state is approached.

Figures 9, 10, and 11 show the results for a 20% break located at a quarter of the duct length from the duct outlet. Because of the off-centered location of the break, the symmetry seen in Figs. 8 and 9 no longer exists. Immediate after the break, the gas velocity jumps up from 44.6 m/s to 106.6 m/s on the left side of the break and drops from 44.6 m/s to -17.7 m/s on the right side as in Fig. 6. The depressurization wave propagates toward the boundaries as before. It takes about 0.0014 s for the disturbance to travel a quarter of the duct length. At

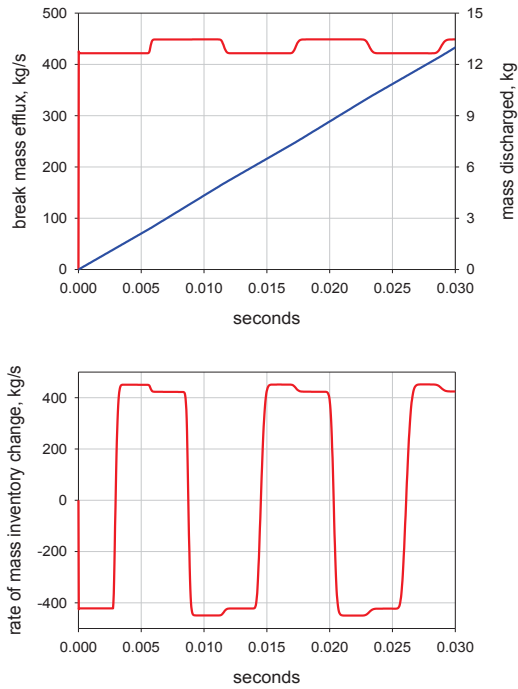


**Figure 8 Break flow, mass discharged, and rate of inventory change - 20% break at mid-length**

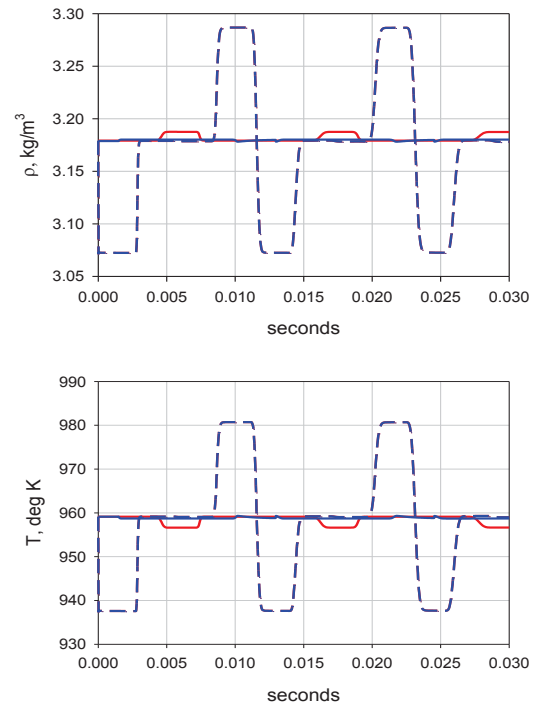


**Figure 10 Mass density and temperature variations - 20% break at quarter-length from outlet**

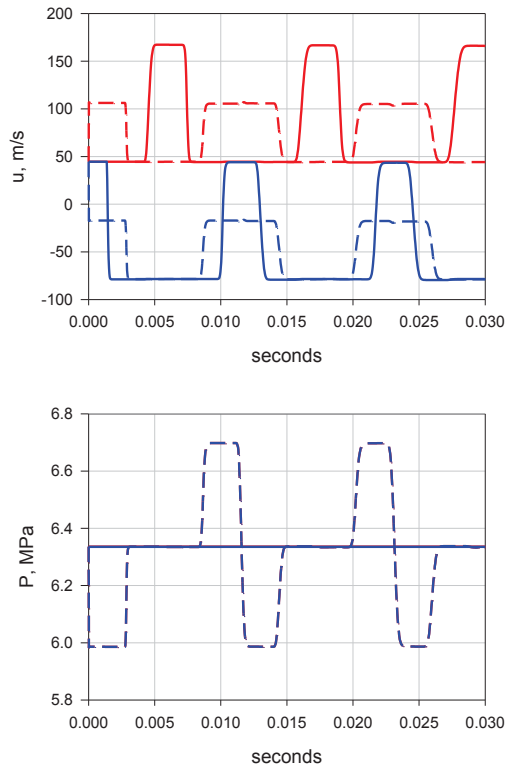


**Figure 9 Velocity and pressure variations - 20% break at quarter-length from duct outlet**

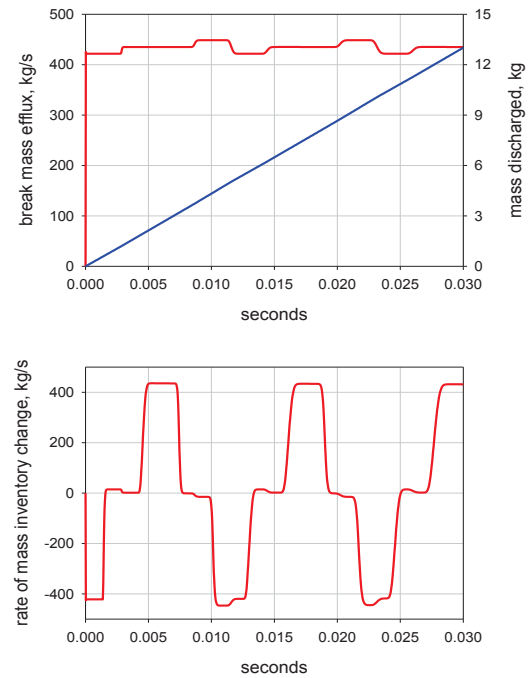


**Figure 11 Break flow, mass discharged, and rate of inventory change – 20% break at quarter-length from outlet**

0.0014 s, the wave reaches the duct outlet. Immediately after that moment and due to the higher pressure at the outlet, the outlet velocity drops from -17.7 m/s to -78.8 m/s. At 0.028 s (0.0014x2), the reflected wave from the outlet arrives at the break location and brings back the outlet pressure and pushes the velocity of the through flow at the break location toward left as shown in Fig. 9. At 0.0042 s (0.0014x3), the wave reaches the inlet. The higher inlet pressure increases the inlet velocity to 167.3 m/s at that instant and remains at that magnitude until the wave reflected from the duct outlet earlier reaches the inlet at 0.007 s (0.0014x5) and bring the inlet velocity back to 44.6 m/s.

The pressure at the break is initially lowered to 5.98 MPa but restored to 63.4 MPa by the wave reflected from the duct outlet. It remains at that level until 0.0084 s (0.0014x6) when the first reflected wave from the inlet brings additional flow to the break location and raises the pressure there to 6.70 MPa. This pressure persists for 0.0028 s (0.0014x2) until the reflected waves from the boundaries arrive at the break location again.

It is apparent that tracking the waves manually becomes tedious very quickly. However, based on the tracking described above, it is clear that the MOC model does track the waves correctly and can be relied on to keep track of all the waves at all times.

Simulations were made for smaller breaks (5 and 10%) at mid-and quarter-length. The same set of waves is induced in each case. The timing is the same but the wave amplitude is less. For smaller breaks the through-flow in the duct remains positive and the flow reversal seen for the 20% break did not occur. It is found that the pressure drop, density change, and break flow rate are not sensitive to the break location despite the different wave patterns discussed above. As expected, smaller break results in smaller excursions in pressure, gas velocity, and mass density.

Only a brief time period after the break is simulated where the conditions at lower plenum of the reactor vessel (duct inlet) and the steam generator (duct outlet) can be assumed constant. This brief time period contains several cycles of oscillations and is sufficiently long to yield useful information. The numerical model can be used to simulate longer time periods of transients if the thermodynamic states in the lower plenum and in the steam generator are known over an extended period.

## CONCLUSIONS

This study has demonstrated that all the primary variables of interest such as the flow, pressure wave behavior, system depressurization rate, and the thermodynamic properties in the vicinity of a break in the VHTR hot duct with choked flow can be systematically quantified using the method of characteristics. The next stage in the analysis progression

is to evaluate the break behavior over an extended time period properly accounting for the pressure wave interactions, as well as the pressure changes, in the remainder of the system. Analysis of the system behavior during the depressurization is important not only because the imposed force loadings throughout the system must be accurately considered, but also because this stage of the scenario provides the initial and boundary conditions for the density-gradient flow phase in which air ingress must be evaluated.

## REFERENCES

1. Bechtel National Inc., Combustion Engineering, DOE EG&G Idaho, Inc., GA technologies, Inc., General Electric Company, Oak Ridge National Laboratory, Stone & Webster Engineering Corp., 1992 (issue year), Preliminary Safety Information Document for the Standard MHTGR, HTGR-86-024.
2. Zucrow M. J., and Hoffman, J. D., Vols. 1 and 2. 1976 and 1977, Gas Dynamics, Volumes 2, John Wiley and Sons, Inc.
3. Denton, G. S., 2009, CFD Simulation of Highly Transient Flows, Ph.D. thesis, University College London.
4. Peterson, H., 1970, The Properties of Helium: Density, Specific Heats, Viscosity, and Thermal conductivity at Pressure from 1 to 100 bar and from room temperature to about 1800 K, Riso Report No. 224, Danish Atomic Energy Commission Research Establishment.
5. Laney, C. B., 1998, Computational Gasdynamics, Cambridge University Press.
6. Moody, F. J., 1990, Introduction to Unsteady Thermofluid Mechanics, John Wiley and Sons, Inc.
7. Oke, A., Mahegerefteh, H., Economou, I., and Rykov, Y., 2003, A Transient Outflow Model for Pipeline Rupture, Chemical Engineering Science, Vol. 58, pp 4591-4604.
8. Atti, O., 2006, Modeling Outflow and Low Temperature Induced Crack Propagation in Pressurized Pipelines, PhD thesis, University College London.
9. Wylie, E. B., and Streeter, V. L., 1993, Fluid Transients in Systems, Prentice Hall.